



Cite this: *Polym. Chem.*, 2020, **11**, 304

Received 7th October 2019,
Accepted 29th October 2019

DOI: 10.1039/c9py01510h

rsc.li/polymers

Thermo-responsive 3D-printed polyrotaxane monolith†

Qianming Lin,  Miao Tang and Chenfeng Ke *

Thermo-responsive 3D-printed hydrogels that are composed of methylated α -cyclodextrin polyrotaxanes have been synthesized through post-3D-printing methylation. With a high methylation degree of the threaded α -cyclodextrins, the fabricated monolith exhibits a two-stage thermo-induced aggregation behavior, in which a second micro-crystallization process was identified for the first time. The methylated polyrotaxane monoliths possess reversible temperature-dependent size, transparency, and elastic moduli switching in an aqueous environment. Through dual-material 3D printing, the 3D-printed monolith actuates back-and-forth at different temperatures.

Since the discovery of α -cyclodextrin (α -CD) and polyethylene glycol (PEG)-based polypseudorotaxane and polyrotaxanes,¹ a number of functional materials have been derivatized from these CD-based polyrotaxane systems.² For example, by covalently linking adjacent α -CD rings on a polyrotaxane, Harada *et al.* synthesized α -CD nanotubes after dethreading the PEG.³ Ito *et al.* developed a series of 'slide-ring' materials⁴ through crosslinking α -CD rings between polyrotaxanes to form movable crosslinkers. These slide-ring materials exhibit outstanding mechanical properties⁵ and have been commercialized as anti-scratching coatings.⁶ When high molecular weight PEG is employed as the axle, upon α -CD threading, a viscoelastic hydrogel is formed,⁷ which has been demonstrated for drug and gene delivery applications.⁸ In these α -CD polypseudorotaxane hydrogels, the polypseudorotaxanes pack to form hexagonal microcrystalline domains^{9,10} *via* water-mediated hydrogen-bonding networks, where, upon mechanical agitation, the hydrogen-bonded microcrystalline domains deform and reform dynamically. Taking advantage of the reversible nature of these microcrystalline domains, we recently introduced α -CD-based polypseudorotaxane hydrogels as direct-ink-writing (DIW) 3D printing inks and successfully

fabricated a series of hydrogel monoliths composed of polyrotaxanes.^{11,12} When the hydrogen-bonding interactions between α -CD rings are disrupted and re-established (*via* solvent or pH change), the 3D-printed monolith performs macroscopic work by amplifying the nanoscopic ring-shuttling motions cohesively. In these systems, the designed and 3D-printed hollow lattice architecture creates multiple diffusion paths, which greatly accelerate the macroscopic responsiveness of these polyrotaxane hydrogels to solvent and pH variations.

Compared to the aforementioned chemically switched polyrotaxane hydrogels, developing thermally switchable polyrotaxane hydrogel not only takes advantage of molecular level ring motions but also eliminates the requirement of constructing delicate diffusion paths in 3D-printed architectures. At the molecular level, the thermo-triggered switching of α -CD ring motions in a polyrotaxane¹³ will be fast, compared to those in conventional thermo-responsive polymers (*e.g.* poly-*N*-isopropylacrylamide (PNIPAM)), because the ring motion possesses low kinetic energy barrier compared to the coil-globule transition of PNIPAM.¹⁴ It has been reported that,^{15,16} when the hydroxyl groups of α -CDs in polyrotaxane were methylated, the methylated polyrotaxane exhibits a thermo-responsive sol-gel transition in an aqueous environment. At a higher temperature, the methylated α -CDs aggregate *via* van der Waals interaction, forming supramolecular crosslinks to afford a hydrogel. However, these methylated polyrotaxanes are synthesized through the methylation of native CD-based polyrotaxanes, because it is challenging to thread methylated α -CDs onto PEG to form a polypseudorotaxane.¹⁷ Furthermore, the methylation of the hydroxyl groups of α -CDs will also dismantle the hydrogen-bonded microcrystalline domains that are critical for DIW 3D printing.¹⁸ Hence, the most promising path to preserve the 3D printability of the ink and introduce methylated α -CD-based polyrotaxanes into 3D-printed materials is the methylation of native CD-based polyrotaxane monoliths. Herein, we report a post-3D-printing methylation method to prepare methylated α -CD polyrotaxane monoliths with designed 3D architectures at the macroscopic level and

Department of Chemistry, Dartmouth College, 6128 Burke Laboratory, Hanover, New Hampshire, 03755, USA. E-mail: chenfeng.ke@dartmouth.edu

†Electronic supplementary information (ESI) available. See DOI: 10.1039/c9py01510h

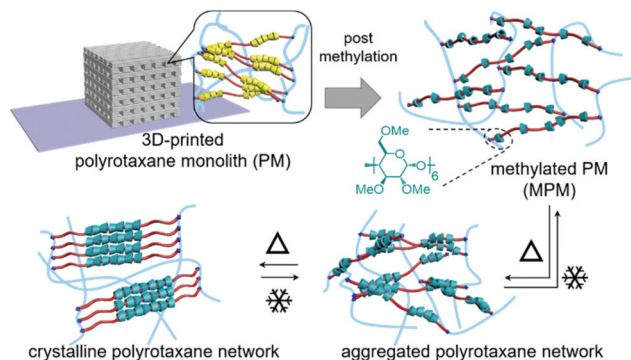


Fig. 1 Graphical illustration of the post 3D-printing methylation of a polyrotaxane monolith, and the molecular level α -CD ring transitions in the thermally responsive methylated α -CD-based polyrotaxane monoliths at different temperatures.

desired methylation degrees at the molecular level (Fig. 1). These 3D-printed monoliths exhibit temperature-dependent size change, transparency variation and elastic moduli switching, which is attributed to the thermo-triggered α -CD ring motions switching among a randomly shuttling state, an aggregated state, and a crystalline state. In particular, the permethylated α -CD polyrotaxane monolith exhibits a two-stage thermo-triggered aggregation (Fig. 1). Through dual-material 3D printing and coupling with a conventional hydrogel, this temperature-controlled ring motion is amplified to the macro-scale, actuating a 3D-printed bilayer monolith bent back-and-forth between 4 °C to 90 °C.

To introduce methylated α -CDs into 3D-printed polyrotaxane monoliths, post-printing methylation of the native α -CD-based polyrotaxane monolith (PM) was chosen in this investigation. Firstly, native α -CD-based PMs were fabricated using

our previously reported method,¹² and the freshly prepared PM hydrogels were exchanged to a DMSO-gel for methylation. In DMSO, the PM-gel swells, which enables the reactive reagents to access the hydroxyl groups of α -CDs throughout the 3D-printed monolith (Fig. S11†). When the PM DMSO-gel was introduced with potassium *tert*-butoxide (*t*-BuOK) for deprotonation, it deswelled significantly and became less transparent. It is also noticeable that the soft PM DMSO-gel was converted to a more rigid monolith in the presence of an excess of *t*-BuOK (0.75–32 equiv. to $-\text{OH}_{\text{CD}}$, Table S1†). The reaction was gently shaken to preserve the 3D-printed architecture. DMSO solution of MeI (0.75–32 equiv. to $-\text{OH}_{\text{CD}}$, Table S1†) was added. As the methylation proceeded, the shrunk PM^-/K^+ DMSO-gel swelled again and gradually became more transparent. The reaction was quenched in water and washed extensively. To quantify the methylation degree ($n_{(-\text{OMe})}/n_{(\text{OH})_{\text{total}}}$) in the synthesized methylated PMs (MPMs), the MPM hydrogels were hydrolyzed in DCl solution (20 v/v% DCl in D_2O), generating soluble species for ^1H NMR analysis (see ESI†). Experimentally, we recorded large methylation degree variation in parallel reactions (Table S1†), which may come from the de-swelling of the deprotonated PM^-/K^+ DMSO-gel, which hindered a thorough diffusion of *t*-BuOK.

To consistently methylate the hydroxyl groups of CDs and control their methylation degree, PM hydrogels were deprotonated in NaOH aqueous solutions, and the opaque PM hydrogels were converted to transparent PM^-/Na^+ hydrogels, followed by a solvent exchange to DMSO-gels (Fig. 2a). The elastic moduli of PM^-/Na^+ hydrogel ($G' = 210$ Pa) increased to PM^-/Na^+ DMSO-gel of $G' = 82\,000$ Pa (Fig. S10†), suggesting that DMSO poorly solvates the deprotonated α -CD rings. When MeI was added, the synthesized methylated α -CDs are well-solvated by DMSO, which enabled the diffusion of MeI into the mono-

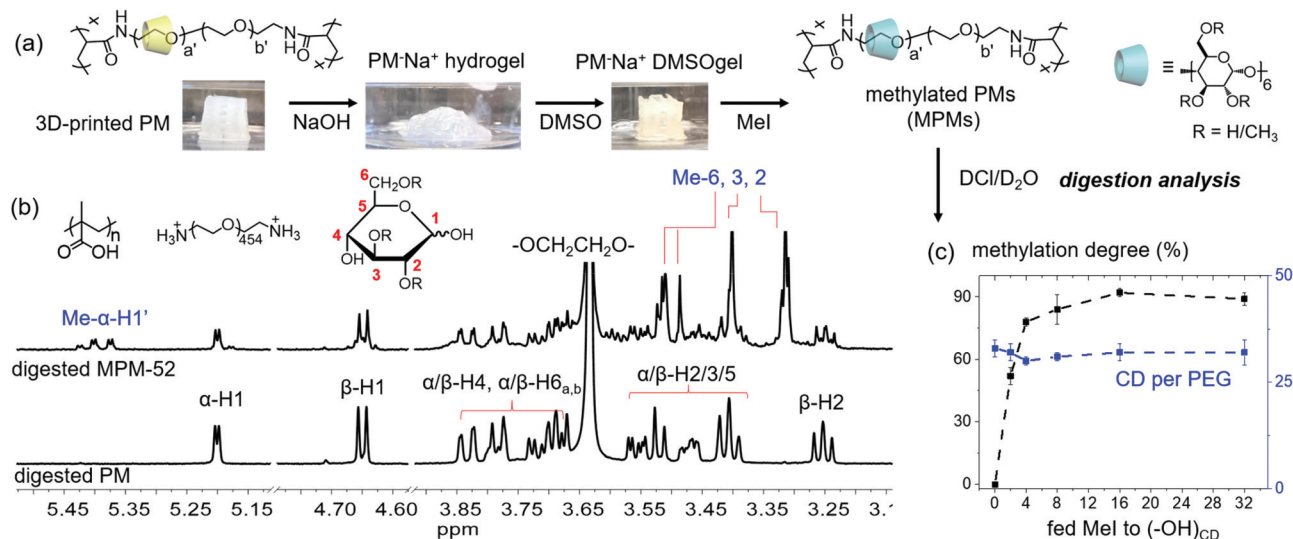


Fig. 2 (a) Post-printing synthesis of methylated polyrotaxane monoliths (MPMs) and their hydrolyzed products in DCl/ D_2O . (b) ^1H NMR spectra of the digested products of PM and MPM in DCl/ D_2O at 298 K. (c) Averaged methylation degrees (black square, calculated from three parallel experiments) of MPMs obtained through post-printing methylation with different feeding MeI ratios. The numbers of α -CDs per PEG in MPMs (blue square) were also calculated from the ^1H NMR spectra.

lith for subsequent methylation. The synthesized MPMs were subjected to ^1H NMR digestion analysis (Fig. 2b and c) to afford soluble PEG, α - and β -methylglucopyranose, and poly(methylacrylic acid). The methylation degrees of the obtained MPMs could be controlled very well, which were calculated by comparing the integrations of proton resonance of methyl groups (3.32, 3.40 and 3.51 ppm) to H-1 of glucose (5.39, 5.20, and 4.65 ppm, Fig. 2b). When three feeding amounts of MeI (Fig. 2c and Table S2†) were tested, MPMs possessing methylation degrees of $52 \pm 4\%$, $78 \pm 2\%$, and $92 \pm 2\%$ were consistently prepared, which are noted as MPM-52, MPM-78, and MPM-92, respectively. The hydroxyl groups (OH-2,3,6) at the primary and secondary faces of α -CD were methylated statistically, as shown in Fig. 2b. The average number of α -CD threaded on PEG remains unchanged during the post-printing methylation (33 ± 3 α -CDs per PEG, Fig. 2c, and Table S2†).

In these synthesized MPM hydrogels, the hydrogen bonding interactions between the α -CD rings were disrupted, and these α -CDs shuttle along the PEG axles. Increasing the temperature of the hydrogel dehydrates the methylated α -CDs, inducing the aggregation of the rings in the polyrotaxane. This temperature-induced aggregation will trigger a simultaneous switching of the rings' random shuttling state to stationary state. At bulk, this synchronized ring motion will result in a fast temperature-dependent elastic moduli change for actuation (Fig. S14–16†).

To investigate the temperature-dependent properties of MPMs, thin disks of MPM hydrogels were prepared and their diameters (Fig. 3a) were recorded at different temperatures in water. The diameter (d_t) of MPM-52 hydrogel recorded at 90°C decreased by 22% compared to its diameter (d_0) at 4°C . The temperature-dependent deswelling of the hydrogel became more significant for MPMs with higher methylation degrees, and MPM-78 and MPM-92 shrunk by 41% and 52%, respectively, after being heated to 90°C . These MPM thin disks† were subjected to frequency-dependent rheological investigations firstly at 4°C . Compared to PM hydrogel, MPM hydrogels exhibit frequency-dependent elastic moduli, which are measured less than 200 Pa at low shear frequency and increased significantly at high shear frequency (Fig. 3b). The

frequency-dependent moduli of MPMs recorded at 4°C suggests the methylated α -CDs in the MPM interact through van der Waals interaction even below the reported sol-gel transition temperature of methyl- α -CD-based polyrotaxanes.¹⁹ This could be attributed to the close proximity of methylated α -CDs in the crosslinked polyrotaxane network. Increasing the temperature from 4°C to 85°C , the G' of MPM-52 increased modestly (black square, Fig. 3c), compared to the strongly temperature-dependent G' of MPM-78 (blue dot) and MPM-92 (red triangle). Upon heating, the elastic moduli of MPM-78 increased nearly linearly to $G' = 440$ Pa at 85°C . The elastic moduli of MPM-92 hydrogel quickly reached a plateau from 160 Pa (4°C) to 290 Pa (25°C) at the critical gelation temperature of permethyl- α -CD polyrotaxanes.¹⁵ Interestingly, a second stage elastic moduli increase was recorded between 70 – 85°C , with $G' = 750$ Pa at 85°C (Fig. 3c). The rapidly increased elastic moduli between 70 – 85°C suggest that a denser supramolecular crosslinking network was formed.

To investigate the two-stage temperature-dependent aggregation behavior of these methylated α -CDs in MPMs, MPM xerogels were prepared at 4°C and 90°C (see ESI† for details), respectively, for powder X-ray diffraction (PXRD) analysis. PM packed to form hexagonal cylinders²⁰ in the solid-state with diffractions observed (Fig. 4a) at $2\theta = 12.7^\circ$ (100), 19.6° (210), and 22.3° (300), respectively. Similar broad diffraction peaks with $2\theta = 12.9^\circ$, and 20.2° were recorded in MPM-52 xerogel prepared at 4°C , and a new diffraction peak at 8.8° was observed (Fig. 4b, dashed line). PXRD profiles of MPM-78 and MPM-92 xerogels obtained at 4°C (Fig. 4c and d, dashed line) are similar to that of MPM-52 and those of methylated α -CD polyrotaxane gels.^{15,16} In contrast, PXRD profiles of MPM-78 and MPM-92 xerogels recorded at 90°C possess strong diffraction peaks in the solid-state. Specifically, new diffraction peaks of $2\theta = 8.1^\circ$, 8.8° , 13.1° , 15.4° , 19.9° , 21.5° , 22.6° , and 24.0° were recorded in MPM-92 xerogel (Fig. 4d, solid line). Our attempt to index these diffractions to a crystalline unit cell was unsuccessful, which may due to the co-existence of several polymorphs. The crystalline domain correlation mean sizes of MPM-92 were calculated from the diffraction peaks $2\theta = 8.8^\circ$ as 3.2 nm at 4°C and 8.6 nm at 90°C respectively, according to the Scherrer equation (see ESI† for details). The highly

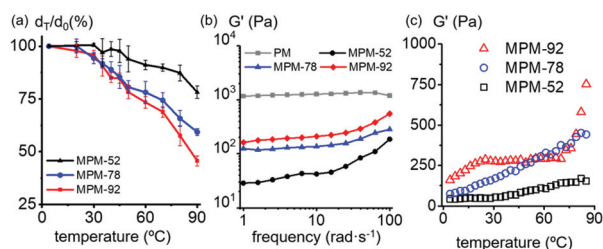


Fig. 3 (a) Averaged deswelling ratios (d_t/d_0) of MPM-52 (black triangle), MPM-78 (blue circle) and MPM-92 (red rectangular) at different temperatures. The fully swelled diameters of thin disks measured at 4°C are set as d_0 . (b) Frequency sweeps of elastic moduli (G') of PM, MPM-52, MPM-78, MPM-92, respectively at 4°C ; (c) temperature-dependent elastic moduli (G') of MPM-52, MPM-78, and MPM-92 recorded at a shear frequency of 1 rad s^{-1} between 4°C and 90°C .

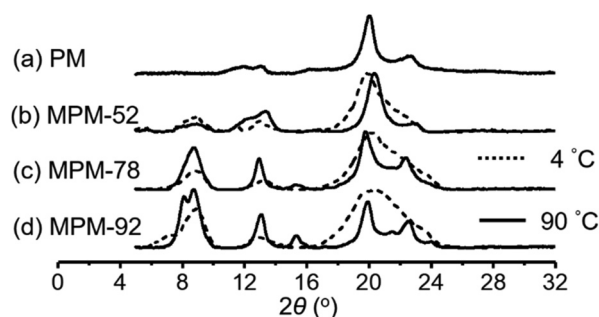


Fig. 4 Wide-angle PXRD profiles of (a) PM, (b) MPM-52, (c) MPM-78, and (d) MPM-92 xerogels prepared at 4°C (dashed line) and 90°C (solid line), respectively.

ordered solid-state superstructures of nearly permethylated α -CD polyrotaxane in MPM-92 xerogel obtained at 90 °C suggests the polyrotaxanes further refined their packing at a higher temperature, resulting in a second stage elastic moduli enhancement in the temperature-dependent rheology investigations. To the best of our knowledge, this is the first observation of a highly crystalline phase formed by methylated α -CD polyrotaxane. At a higher temperature, it is reported that the hydration number of each repeating unit EG (number of H₂O to solvate EG) is reduced by 50%.²¹ The dehydration of PEG axles provided a more hydrophobic environment for the further crystallization of permethylated α -CD polyrotaxanes in MPM-92. Furthermore, we suggest a “pre-refinement” effect during the synthesis of MPM-92, because highly crystalline native α -CD polyrotaxanes are pre-formed in PM. This refined local structure subsequently improved the crystallinity of the aggregated permethylated α -CD polyrotaxanes in MPM-92.

The formation and deformation of the highly crystalline form of permethylated α -CD polyrotaxane in MPM-92 gel is highly reversible. As shown in Fig. 5a and Movie S1,[†] when an opaque MPM-92 hydrogel at 90 °C was transferred to an ambient environment, within 10 seconds, the hydrogel turned to transparent as a result of the deformation of the crystalline domain. The transparency change is significantly faster than a traditional PNIPAM plate fabricated in a similar manner (40–50 seconds, Fig. S22[†]), which could be attributed to the fast and synchronized ring motions in the polymer network from the crystalline state to loosely aggregated state.

The temperature-dependent (de)swelling and transparency switching of MPM-92 enables the construction of temperature-responsive soft actuators. As shown in Fig. 5b, a transparent MPM-92-based sea star (left) swelled in water at 4 °C. Upon heating, both the size and opacity changed gradually. When MPM is coupled with a conventional thermo-inert hydrogel, temperature-triggered directional motion could be realized through the design of 3D-printed bilayer structures (Fig. 5c). In this design, two directional α -CD-based hydrogels were printed on top of a dimethylacrylamide (DMA)-based hydrogel (see ESI[†] for the preparation of the crosslinked PDMA hydrogel). After photo-crosslinking and post-printing methylation, these bilayer hydrogel monoliths were obtained, in which the top layers are composed of MPM-92 (dry mass: 33.0 mg, Fig. 5c, left) and the bottom layers are composed of PDMA (dry mass: 36.0 mg, Fig. 5c, left). At 4 °C, the MPM-92 swelled to bend the monoliths downwards (top, Fig. 5c). Upon heating to 45 °C, the swelling ratio of MPM-92 and PDMA matched, and the monoliths turned to flat sheets (middle). When keep heating the monoliths to 90 °C, the bilayers bent upwards (down) as a result of the deswelling of the MPM-92 hydrogels and increased elastic moduli. This thermally triggered bending actuation could be controlled by designing their 3D-printing patterns, *e.g.* different degrees of bending when the top layers were printed into vertical or horizontal patterns. For example, the bilayer monolith with a longer aspect ratio pattern of MPM-92 (Fig. 5c, left) bent 1.09 g/g of crosslinked PDMA backward around 270° upon heating from 4 °C to 90 °C. The

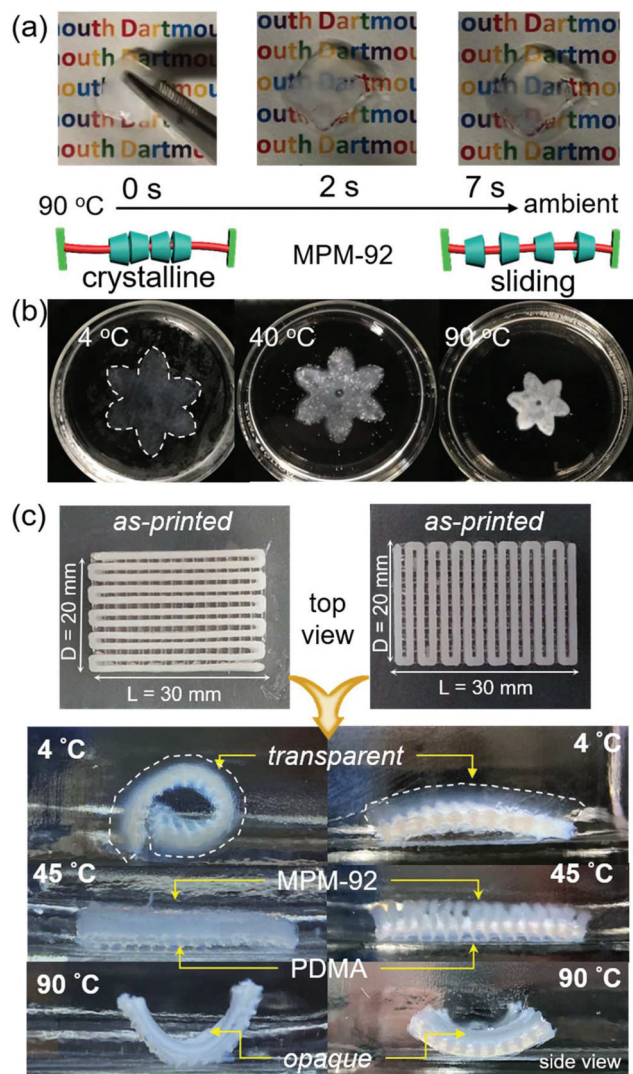


Fig. 5 (a) Rapid opacity change of MPM-92 after removing the thin plate from 90 °C heating chamber and placed it at ambient environment on a glass slide. (b) The temperature-dependent size and opacity change of a 3D-printed sea star in an aqueous environment. (c) Temperature-induced shape morphing of two bilayer monoliths, in which the top layer is constructed by MPM-92 and the bottom layer is constructed by crosslinked PDMA.

bending motions (Movie S2[†]) have been repeated five times in an aqueous environment, demonstrating the highly reversible nature of the ring motion-triggered macroscopic shape morphing.

In summary, a series of 3D-printed methylated α -CD-based polyrotaxane hydrogels were prepared *via* a post-printing methylation method. Compared to the solution phase synthesis, the (de)swelling state of the monolith critically determines the reaction consistency of the post-printing methylation, and thorough methylation of the 3D-printed monolith is achieved using a matching (de)swelling solvent. At varied methylation degrees, the prepared MPM hydrogels exhibit different thermo-responsive behavior. Specifically, the

MPM-92 hydrogel exhibits a two-stage thermo-triggered aggregation-followed-by-crystallization process, which is confirmed by rheological studies and PXRD measurements. At a high-temperature range (70–90 °C), MPM-92 responds to the thermo-fluctuation very rapidly by changing its elastic moduli, macroscopic size and opacity, as a result of the synchronized polyrotaxane reorganization in the crosslinked polymer network. Through the coupling with a conventional hydrogel and dual-material 3D printing, these thermo-responsive properties are amplified as macroscopic bending motions in aqueous environment at different temperatures. Our results suggest a different path to access dynamic mechanically interlocked systems through post-printing modification in 3D-printed architecture and demonstrate the fabrication of temperature-responsive thermo-actuation prototypes for soft robotic applications.

Conflicts of interest

The authors declare no competing financial interest.

Acknowledgements

Q. L., C. K. acknowledge the funding support from NSF EPSCoR New Hampshire Bio-Made Center (No. 1757371). M. T., C. K. thank the support of the Beckman Young Investigator Program. We thank Prof. Kohzo Ito and Dr. Rina Maeda at the University of Tokyo for helpful discussions.

Notes and references

‡The MPMs obtained at 90 °C were employed for rheological measurements (their water content remains constant between 4–90 °C).

- 1 A. Harada, J. Li and M. Kamachi, *Nature*, 1992, **356**, 325–327.
- 2 G. Wenz, B.-H. Han and A. Müller, *Chem. Rev.*, 2006, **106**, 782–817.
- 3 A. Harada, J. Li and M. Kamachi, *Nature*, 1993, **364**, 516–518.
- 4 Y. Okumura and K. Ito, *Adv. Mater.*, 2001, **13**, 485–487.
- 5 A. B. Imran, K. Esaki, H. Gotoh, T. Seki, K. Ito, Y. Sakai and Y. Takeoka, *Nat. Commun.*, 2014, **5**, 5124.
- 6 K. Mayumi, K. Ito and K. Kato, *Polyrotaxane and sliding materials*, Royal Society of Chemistry, Cambridge, 2015.
- 7 J. Li, A. Harada and M. Kamachi, *Polym. J.*, 1994, **26**, 1019–1026.
- 8 G. Liu, Q. Yuan, G. Hollett, W. Zhao, Y. Kang and J. Wu, *Polym. Chem.*, 2018, **9**, 3436–3449.
- 9 S. Uenuma, R. Maeda, H. Yokoyama and K. Ito, *Macromolecules*, 2019, **55**, 4158–4161.
- 10 S. Uenuma, R. Maeda, H. Yokoyama and K. Ito, *Chem. Commun.*, 2019, **55**, 4158–4161.
- 11 Q. Lin, X. Hou and C. Ke, *Angew. Chem., Int. Ed.*, 2017, **56**, 4452–4457.
- 12 Q. Lin, L. Li, M. Tang, X. Hou and C. Ke, *J. Mater. Chem. C*, 2018, **6**, 11956–11960.
- 13 H. Kojima and T. Koga, *Macromolecules*, 2016, **49**, 7015–7024.
- 14 X. Wang, X. Qiu and C. Wu, *Macromolecules*, 1998, **31**, 2972–2976.
- 15 M. Kidowaki, C. Zhao, T. Kataoka and K. Ito, *Chem. Commun.*, 2006, 4102–4103.
- 16 T. Karino, Y. Okumura, C. Zhao, M. Kidowaki, T. Kataoka, K. Ito and M. Shibayama, *Macromolecules*, 2006, **39**, 9435–9440.
- 17 T. Higashi, J. Li, X. Song, J. Zhu, M. Taniyoshi, F. Hirayama, D. Iohara, K. Motoyama and H. Arima, *ACS Macro Lett.*, 2016, **5**, 158–162.
- 18 L. Li, Q. Lin, M. Tang, A. J. Duncan and C. Ke, *Chem. – Eur. J.*, 2019, **25**, 10768–10781.
- 19 T. Kataoka, M. Kidowaki, C. Zhao, H. Minamikawa, T. Shimizu and K. Ito, *J. Phys. Chem. B*, 2006, **110**, 24377–24383.
- 20 I. N. Topchieva, A. E. Tonelli, I. G. Panova, E. V. Matuchina, F. A. Kalashnikov, V. I. Gerasimov, C. C. Rusa, M. Rusa and M. A. Hunt, *Langmuir*, 2004, **20**, 9036–9043.
- 21 T. Shikata, M. Okuzono and N. Sugimoto, *Macromolecules*, 2013, **46**, 1956–1961.